ARTICLES SCIENCE CHINA Materials

mater.scichina.com link.springer.com

Published online 19 September 2019 | https://doi.org/10.1007/s40843-019-9585-3

*Sci China Mater* 2020, 63(2): 300–306

# High-entropy alumino-silicides: a novel class of high-entropy ceramics

Tongqi Wen[1,2†], Honghua Liu[1†], Beilin Ye[1], Da Liu[1] and Yanhui Chu[1*]

**ABSTRACT** **High-entropy ceramics (HECs) are gaining significant interest due to their huge composition space, unique microstructure, and adjustable properties. Previously reported studies focus mainly on HECs with the multi-cationic structure, while HECs with more than one anion are rarely studied. Herein we reported a new class of HECs, namely high-entropy alumino-silicides $(Mo_{0.25}Nb_{0.25}Ta_{0.25}V_{0.25})(Al_{0.5}Si_{0.5})_2$ (HEAS-1) with multi-cationic and -anionic structure. The formation possibility of HEAS-1 was first theoretically analyzed from the aspects of thermodynamics and lattice size difference based on the first-principles calculations and then the HEAS-1 were successfully synthesized by the solid-state reaction at 1573 K. The as-synthesized HEAS-1 exhibited good single-crystal hexagonal structure of metal alumino-silicides and simultaneously possessed high compositional uniformity. This study not only enriches the categories of HECs but also will open up a new research field on HECs with multi-cationic and -anionic structure.**

**Keywords:** high-entropy ceramics, alumino-silicides, first-principles calculations, solid solutions

## INTRODUCTION

Since their discovery in 2004, high-entropy alloys (HEAs) have attracted significant research interest for their huge composition space, unique microstructure, adjustable properties, and various potential applications [1,2]. Generally, in a HEA, four or more principal elements can be mixed in near-equiatomic ratios or at least with each element being between 5 at% and 35 at% to generate a maximum molar configurational entropy of $\Delta S_{mix}=R\cdot\ln N$, where $N$ is the number of components and $R$ is the gas constant [1–3]. As a result, HEAs exhibit superior strength and ductility [4], outstanding irradiation resistance [5], good corrosion resistance [6], high fracture toughness [7], interesting creep characteristics [8] and plastic behavior [9]. Inspired by HEAs concept, the concept of high-entropy ceramics (HECs), namely multicomponent ionic compounds, was first proposed in the multicomponent metal oxides in 2015 [10] and then it has been gaining significant interest in recent years. Up to now, extensive efforts have been devoted to exploring the diverse HECs, including metal oxides [10,11], carbides [12–16], diborides [17–19], and silicides [20,21], with wide-ranging applications in the structural and functional fields. These HECs show many superior mechanical, physical and chemical performances, such as high hardness and modulus, low thermal conductivity, good thermodynamics stability and corrosion resistance, superior electrochemical and physicochemical properties [10–14,16,17,22,23]. Unlike HEAs, whose structures consist of a single lattice occupied by metal elements [1,2], the structures of HECs involve a cationic sublattice and an anionic sublattice occupied by metal elements and nonmetallic element, respectively. Consequently, the disorder of the cationic and anionic sites for HECs can contribute to a maximum molar configurational entropy of $\Delta S_{mix} = \Delta S_{cation} + \Delta S_{anion}$, where $\Delta S_{cation}$ and $\Delta S_{anion}$ are the entropy of cationic and anionic site contribution, respectively. As far as we are concerned, the previously reported studies focus mainly on HECs with the multi-cationic structure, while so far there are very few reports on HECs with more than one anion. In other words, only the cationic site contributes to $\Delta S_{mix}$ for the reported HECs since the contribution from the anionic site is zero. It is worth mentioning that a higher $\Delta S_{mix}$ is closely related to much more superior mechanical, physical and chemical properties, especially thermodynamics stability. Therefore, the exploration of new HECs with higher $\Delta S_{mix}$, namely with multi-cationic and -anionic structure, is of great interest

[1] School of Materials Science and Engineering, South China University of Technology, Guangzhou 510641, China
[2] School of Natural and Applied Sciences, Northwestern Polytechnical University, Xi'an 710072, China
† These authors contributed equally to this work.
* Corresponding author (email: chuyh@scut.edu.cn)

  

for the scientific community.

In this work, a new class of HECs, namely high-entropy alumino-silicides $(Mo_{0.25}Nb_{0.25}Ta_{0.25}V_{0.25})(Al_{0.5}Si_{0.5})_2$ (HEAS-1) with multi-cationic and -anionic structure, was reported for the first time. The formation possibility of HEAS-1 was first analyzed from lattice size difference and thermodynamics based on the first-principles calculations and then the HEAS-1 was successfully synthesized by solid-state reaction at 1573 K. In addition, the phase compositions, microstructure, and compositional uniformity of the as-synthesized HEAS-1 were investigated in detail.

## THEORETICAL AND EXPERIMENTAL METHOD

### The first-principles calculations

The Vienna *ab-Initio* Simulation Package (VASP) [24,25] was used to perform first-principles calculations based on density functional theory (DFT) with projected-augmented-waves pseudopotential method within generalized-gradient approximation [26,27]. The most stable crystal structures of the starting materials including Mo, Nb, Ta, V, Si, Al from the Materials Project Database [28] were used as input for full optimization with DFT and the corresponding space groups are listed in Table 1. For the individual metal disilicides, such as $MoSi_2$, $NbSi_2$, $TaSi_2$, and $VSi_2$, they all had the hexagonal *C*40 crystal structure with the space group of $P6_222$ from the Materials Project Database, but only $NbSi_2$ and $TaSi_2$ crystal structures with this space group were the most stable [28]. Meanwhile, Gild *et al.* [20] reported that a high-entropy silicide, namely $(Mo_{0.2}Nb_{0.2}Ta_{0.2}Ti_{0.2}W_{0.2})Si_2$, possessed the aforementioned hexagonal *C*40 crystal structure. In this case, we assumed that the individual metal disilicides, alumino-silicides and high-entropy alumino-silicides all possessed the similar crystal structures with the space group of $P6_222$, as shown in Fig. 1. Here Fig. 1a and b are two alternative views of the hexagonal unit cell showing the ABC stacking sequences. The red balls represent the atoms at the cationic sublattice (Mo, Nb, Ta, or V) and the blue balls stand for the atoms at the anionic sublattice (Al or Si). To mimic the complete chemical disorder at both cationic and anionic sublattice for individual metal alumino-silicides and HEAS-1, the special quasi-random structure (SQS) approach [29] was adopted to construct the structures. To be specific, the Alloy Theoretic Automated Toolkit code [30] was utilized to generate the SQS with 36 atoms in which 12 atoms resided at the cation positions and the other 24 atoms occupied the anion positions. For the DFT calculations of energies and lattice parameters in this work, the energy cutoff was 600 eV and the *k*-mesh grid was $2\pi\times1/60$ Å$^{-1}$. Meanwhile, the electronic energy convergence criterion was $10^{-6}$ eV and all structures were relaxed until forces acting on each atom became smaller than 0.01 eV Å$^{-1}$.

### Synthesis of HEAS-1

The commercially available Mo, Nb, Ta, V, Si, and Al powders (99.9% purity, average particle size: 1–3 μm, Shanghai ChaoWei Nanotechnology Co. Ltd., China) were used as starting materials to synthesize HEAS-1. The starting powders were mixed with a ratio of 8.33 mol% Mo, 8.33 mol% Nb, 8.33 mol% Ta, 8.33 mol% V, 33.33 mol% Si, and 33.33 mol% Al, and then milled by hand for 1 h in an agate mortar. Afterwards, they were put into an alumina crucible with an alumina lid and the whole assembly was directly placed inside a horizontal alumina tube furnace. Finally, they were heated from room temperature to 1573 K at a rate of 10 K min$^{-1}$, held for 30 min, and followed by furnace cooling down naturally to room temperature to obtain HEAS-1 powders. The whole heating and cooling process was conducted in flowing Argon gas (99.99%, purity) with a flowing rate of 200 sccm.

### Characterization

The phase composition of the as-synthesized powders was first analyzed by X-ray diffraction (XRD) using Cu Kα radiation (0.15418 nm) (X'pert PRO; PANalytical, Netherlands) operated under a voltage of 40 kV and a current of 40 mA. The equivalent counting time for a

**Table 1** Calculated equilibrium lattice parameters, space group and DFT energies of the ground-state crystal structures of different elementary substances

| Systems | Mo | Nb | Ta | V | Si | Al |
|---|---|---|---|---|---|---|
| Lattice parameters *a* (Å) | 3.163 | 3.308 | 3.319 | 2.997 | 5.463 | 4.039 |
| Space group | $Im\bar{3}m$ | $Im\bar{3}m$ | $Im\bar{3}m$ | $Im\bar{3}m$ | $Fd\bar{3}m$ | $Fm\bar{3}m$ |
| Energies *E* (eV atom$^{-1}$) | −10.935 | −10.216 | −11.814 | −8.992 | −5.424 | −3.747 |

  

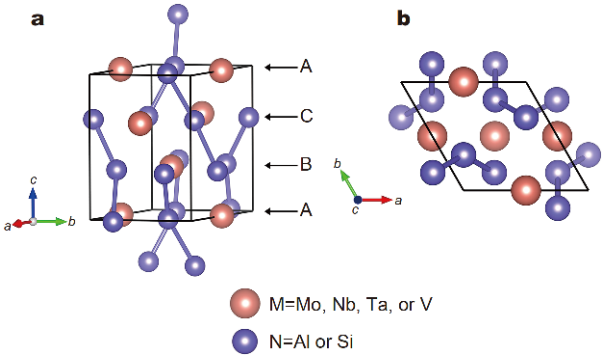


**Figure 1** A simple schematic illustration of the atomic structure that does not take the lattice distortion into account of HEAS-1. (a) and (b) are two alternative views of the hexagonal unit cell showing the ABC stacking sequences.

conventional point detector would be 30 s per point at 0.01° $2\theta$ increments. The morphology, microstructure and compositional uniformity of the as-synthesized products were then characterized by scanning electron microscope (SEM, Supra-55; Zeiss, Germany) and transmission electron microscope (TEM, Tecnai F30G2; FEI, Netherlands) equipped with energy dispersive spectroscopy (EDS). In particular, for TEM characterizations, 2 g powders were dissolved into ethanol, exposed to ultrasound for 10 min and then the clear liquid solution on the surface was dropped on the copper screen with carbon film by pipette.

## RESULTS AND DISCUSSION

In order to analyze the synthesis possibility of HEAS-1, the lattice size difference, $\delta$, an empirical parameter to predict the formation possibility of high-entropy materials [14,16], should be first analyzed. The $\delta$ of HEAS-1 can be calculated by the following equation:

$$\delta = \sqrt{\sum_{i=1}^{n} \frac{n_i}{2}\left[\left(1-\frac{a_i}{\bar{a}}\right)^2+\left(1-\frac{c_i}{\bar{c}}\right)^2\right]}, \quad (1)$$

where $n$ is the metal alumino-silicides component species in the HEAS-1, $n_i$ is the molar fraction of the $i$th individual metal alumino-silicides of HEAS-1, $a_i$ and $c_i$ are the corresponding lattice parameters, and $\bar{a} = \sum_{i=1}^{n} n_i a_i$ and $\bar{c} = \sum_{i=1}^{n} n_i c_i$ are the averaged lattice parameters. In general, the smaller $\delta$ suggests the smaller lattice distortion and finally results in the higher formation possibility of the system. In this case, the calculated $\delta$ of HEAS-1 by using the lattice parameters in Table 2 is 1.893%, which is smaller than that of the reported high-entropy $(Zr_{0.25}Ta_{0.25}Nb_{0.25}Ti_{0.25})C$ carbides (2.959%) [16] and $(Hf_{0.2}Zr_{0.2}Ta_{0.2}Nb_{0.2}Ti_{0.2})B_2$ diborides (2.648%) [19]. This result suggests that HEAS-1 can be synthesized from the aspect of lattice size difference. What's more, the thermodynamics of the possible chemical reactions during HEAS-1 synthesis process should be analyzed in detail. In the current work, the starting materials are composed of Mo, Nb, Ta, V, Si, and Al powders. As a result, the relationship between the standard Gibbs free energy ($\Delta G^{\theta}_{R,T}$) of the possible chemical reactions and temperature ($T$) can be described as follows:

$$\mathrm{Mo + Si + Al \rightarrow Mo(Al_{0.5}Si_{0.5})_2} \quad \Delta G^{\theta}_{R,T} = \Delta G^{(2).}_{\mathrm{mix}}, \quad (2)$$

$$\mathrm{Nb + Si + Al \rightarrow Nb(Al_{0.5}Si_{0.5})_2} \quad \Delta G^{\theta}_{R,T} = \Delta G^{(3).}_{\mathrm{mix}}, \quad (3)$$

$$\mathrm{Ta + Si + Al \rightarrow Ta(Al_{0.5}Si_{0.5})_2} \quad \Delta G^{\theta}_{R,T} = \Delta G^{(4).}_{\mathrm{mix}}, \quad (4)$$

$$\mathrm{V{+}Si + Al \rightarrow V(Al_{0.5}Si_{0.5})_2} \quad \Delta G^{\theta}_{R,T} = \Delta G^{(5).}_{\mathrm{mix}}, \quad (5)$$

**Table 2** Calculated equilibrium lattice parameters, DFT energies, mixing enthalpy, mixing entropy, and the lattice size difference of the generated HEAS-1 and four individual metal alumino-silicides at 0 K and 0 Pa by chemical reaction ($n$)

| System | HEAS-1 | $Mo(Al_{0.5}Si_{0.5})_2$ | $Nb(Al_{0.5}Si_{0.5})_2$ | $Ta(Al_{0.5}Si_{0.5})_2$ | $V(Al_{0.5}Si_{0.5})_2$ |
|---|---|---|---|---|---|
| Lattice parameter $a$ (Å) | 4.811 | 4.711 | 4.926 | 4.919 | 4.692 |
| Lattice parameter $c$ (Å) | 6.703 | 6.749 | 6.770 | 6.748 | 6.545 |
| Energies $E$ (eV atom$^{-1}$) | −6.888 | −7.082 | −6.848 | −7.321 | −6.368 |
| Mixing enthalpy $\Delta H^{(n)}_{\mathrm{mix}}$ (kJ mol$^{-1}$) | 1.616 ($n$=6) −32.285 ($n$=7) | −36.664 ($n$=2) | −37.221 ($n$=3) | −31.454 ($n$=4) | −30.264 ($n$=5) |
| Mixing entropy $\Delta S^{(n)}_{\mathrm{mix}}$ | 0.462$R$ ($n$=6) 0.924$R$ ($n$=7) | 0.462$R$ ($n$=2) | 0.462$R$ ($n$=3) | 0.462$R$ ($n$=4) | 0.462$R$ ($n$=5) |
| Lattice size difference $\delta$ (%) | 1.893 | N/A | N/A | N/A | N/A |

$$\frac{1}{4}\mathrm{Mo(Al_{0.5}Si_{0.5})_2}+\frac{1}{4}\mathrm{Nb(Al_{0.5}Si_{0.5})_2}+\frac{1}{4}\mathrm{Ta(Al_{0.5}Si_{0.5})_2}+\frac{1}{4}\mathrm{V(Al_{0.5}Si_{0.5})_2}\rightarrow \mathrm{(Mo_{0.25}Nb_{0.25}Ta_{0.25}V_{0.25})(Al_{0.5}Si_{0.5})_2}$$
$$\Delta G^{\theta}_{R,T}=\Delta G^{(6)}_{\mathrm{mix}}; \quad (6)$$

$$\frac{1}{4}\mathrm{Mo}+\frac{1}{4}\mathrm{Nb}+\frac{1}{4}\mathrm{Ta}+\frac{1}{4}\mathrm{V{+}Si{+}Al}\rightarrow \mathrm{(Mo_{0.25}Nb_{0.25}Ta_{0.25}V_{0.25})(Al_{0.5}Si_{0.5})_2} \quad (7)$$
$$\Delta G^{\theta}_{R,T}=\Delta G^{(7)}_{\mathrm{mix}},$$

where $\Delta G^{(n)}_{\mathrm{mix}}$ is the mixing Gibbs free energy of the chemical reaction ($n$) and can be calculated by the following equation:

$$\Delta G^{(n)}_{\mathrm{mix}}=\Delta H^{(n)}_{\mathrm{mix}}-T\Delta S^{(n)}_{\mathrm{mix}}, \quad (8)$$

where $\Delta H^{(n)}_{\mathrm{mix}}$ and $\Delta S^{(n)}_{\mathrm{mix}}$ are the calculated mixing enthalpy and mixing entropy of the generated HEAS-1 and four individual metal alumino-silicides by chemical reaction ($n$), respectively. $\Delta H^{(n)}_{\mathrm{mix}}$ can be approximated by its value at 0 K ($\Delta H^{0\,\mathrm{K}(n)}_{\mathrm{mix}}$) which can be calculated by the following equation based on the DFT energies:

$$\Delta H^{0\,\mathrm{K}(n)}_{\mathrm{mix}}=E_{\mathrm{pro}}-\overline{E}_{\mathrm{pre}}, \quad (9)$$

where $E_{\mathrm{pro}}$ represents the ground-state DFT energies of the products, and $\overline{E}_{\mathrm{pre}}$ stands for the averaged ground-state DFT energies of the reactants. The equilibrium lattice parameters and DFT energies of the elementary substances and metal alumino-silicides including HEAS-1 are listed in Tables 1 and 2, respectively. By using the corresponding DFT energies, the $\Delta H^{0\,\mathrm{K}(n)}_{\mathrm{mix}}$ ($n$=2, 3, 4, 5, 6, 7) can be calculated and the results are listed in Table 2. In particular, the $\Delta H^{0\,\mathrm{K}(n)}_{\mathrm{mix}}$ of Reaction (6) is larger than zero, suggesting that HEAS-1 is thermodynamically unstable with respect to the four individual metal alumino-silicides at 0 K and 0 Pa. However, the effect of $\Delta S^{(n)}_{\mathrm{mix}}$ on the thermodynamic stability of the system should also be considered. The calculated $\Delta S^{(n)}_{\mathrm{mix}}$ of the generated HEAS-1 and four individual metal alumino-silicides by chemical reaction ($n$) can be expressed as:

$$\Delta S^{(n)}_{\mathrm{mix}}=\Delta S^{\mathrm{pro}}_{\mathrm{mix}}-\Delta\overline{S}^{\mathrm{pre}}_{\mathrm{mix}}, \quad (10)$$

where $\Delta S^{\mathrm{pro}}_{\mathrm{mix}}$ is the mixing entropy of the products and $\Delta\overline{S}^{\mathrm{pre}}_{\mathrm{mix}}$ is the averaged mixing entropy of the reactants. In addition, the mixing entropy $\Delta S_{\mathrm{mix}}$ for a compound can be expressed as follows [14]:

$$\Delta S_{\mathrm{mix}}=-R\left\{\frac{X}{X+Y}\sum_{i=1}^{N_h}x_i^h\ln\left(x_i^h\right)+\frac{Y}{X+Y}\sum_{i=1}^{N_k}x_i^k\ln\left(x_i^k\right)\right\}, \quad (11)$$

where $R$ is the gas constant, $X$ and $Y$ represent the number of sites in the sublattice $h$ and $k$, respectively, $N_h$ and $N_k$ are the elements species in the sublattice $h$ and $k$, respectively, and $x_i^h$ and $x_i^k$ are the molar fractions of the constituent $i$ in the sublattice $h$ and $k$, respectively. As a result, the calculated $\Delta S^{(n)}_{\mathrm{mix}}$ values of the generated HEAS-1 and four individual metal alumino-silicides by Reaction ($n$) are listed in Table 2. In this case, the thermodynamics analysis results of the possible Reactions (2)–(7) are displayed in Fig. 2a, from which it can be clearly observed that all the reactions can proceed simultaneously above 1000 K because the $\Delta G^{\theta}_{R,T}$ of all the reactions are less than zero. However, the driving force of Reaction (6) is the smallest among all the reactions, which indicates that it is the most difficult one to occur when competing with

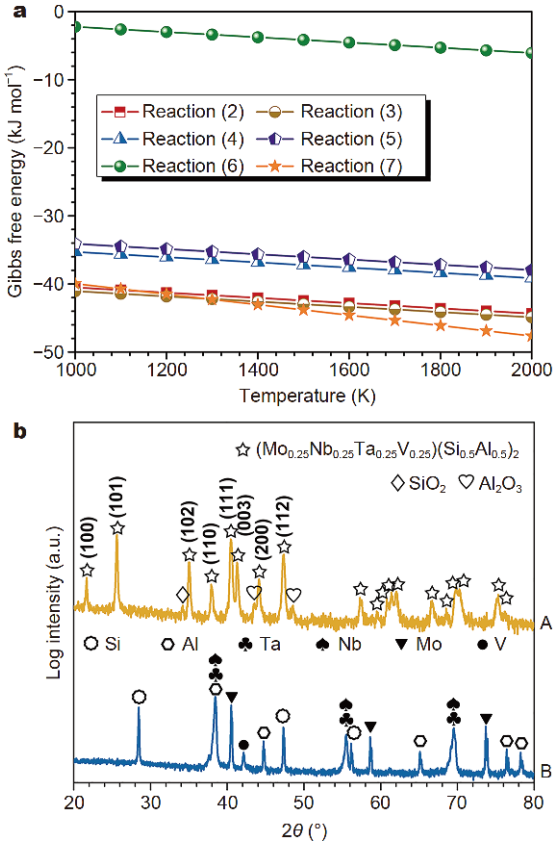


**Figure 2** (a) Thermodynamics analysis of the possible chemical reactions during HEAS-1 synthesis process; (b) XRD patterns: A is for the as-synthesized product and B is for the mixture of the starting materials.

  

other reactions. In addition, it should be noted that the $\Delta G^{\theta}_{R,T}$ of all the reactions show a decrease trend with the increase of the temperature. When the temperature is above 1300 K, Reaction (7) is the most prone to occurring due to its largest driving force among all the reactions. In this case, the synthesis of HEAS-1 through Reaction (7) is very probable from the aspect of thermodynamics. Therefore, in combination of lattice size difference and thermodynamics analysis, the fabrication of HEAS-1 is very probable and worthy to being tried in experiments.

Encouraged by the above comprehensive theoretical analyses, the aforementioned experiment was further performed to attempt to fabricate HEAS-1. Fig. 2b shows the XRD patterns of the mixture of the starting materials (B) and the as-synthesized products (A) on a logarithmic scale. It can be found that a single hexagonal phase of metal alumino-silicides can be clearly seen except for the existence of a small amount of $SiO_2$ and $Al_2O_3$ phases. This suggests that HEAS-1 are successfully synthesized at 1573 K.

To further investigate the morphology, microstructure and compositional uniformity of the as-synthesized HEAS-1, the SEM and TEM characterizations were carried out. Fig. 3a is the typical SEM image of the as-synthesized HEAS-1. It can be obviously observed that the as-synthesized HEAS-1 powders involve numerous irregular particles with the particle sizes of 0.5–3 μm. Fig. 3b, c shows the representative bright-field TEM image and the corresponding selected area electron diffraction (SAED) pattern along zone axis [100] of the as-synthesized HEAS-1, respectively. It can be clearly found that the as-synthesized HEAS-1 exhibit the single-crystal hexagonal structure of metal alumino-silicides because the diffraction spots are arranged in a good symmetry. Fig. 3d is the high-resolution TEM (HRTEM) image, from which we can observe a periodic structure with two sets of fringes with the *d*-space of about 0.432 and 0.342 nm corresponding to {100} and {101} planes of $(Mo_{0.25}Nb_{0.25}Ta_{0.25}V_{0.25})(Al_{0.5}Si_{0.5})_2$ phase, respectively. These are in good agreement with the results (0.417 and 0.354 nm) from first-principles calculations. Moreover, it should be noted that there is an amorphous layer of 2–4 nm on the particle surface, which may be due to the presence of amorphous $SiO_2$. To analyze the element compositions of the as-synthesized HEAS-1, the atomic percentages (at%) of different elements were summarized as follows: Mo (9.35), Nb (10.91), Ta (10.16), V (9.93), Si (29.4), Al (25.69), O (4.56). Clearly, the atomic percentages of Mo, Nb, Ta and V elements in the cationic site are nearly the same and simultaneously the atomic ratio of the cation elements (Mo, Nb, Ta and V) to the anion elements (Al and Si) is around 1:2. Furthermore, the atomic percentage of Si element is much higher than that of Al element, which results from the presence of the higher fraction of $Al_2O_3$ than that of $SiO_2$ in the as-synthesized HEAS-1 (Fig. 2b). Meanwhile, the presence of oxygen element may come from $Al_2O_3$ and $SiO_2$ in the as-synthesized HEAS-1. To investigate the composition uniformity of the as-synthesized HEAS-1, the scanning TEM (STEM)-EDS analysis was further carried out at a collection time of 230 s and an acceleration voltage of 200 kV and the results are displayed in Fig. 3e. The distribution of all elements, including Mo, Nb, Ta, V, Si and Al, is very uniform without evident localization or segregation. In combination with the results from XRD, SEM, and TEM analyses, the HEAS-1 have been successfully synthesized at 1573 K.

## CONCLUSION

In conclusion, a new class of HECs, namely HEAS-1 with multi-cationic and -anionic structure, was reported for the first time. We first theoretically demonstrated the

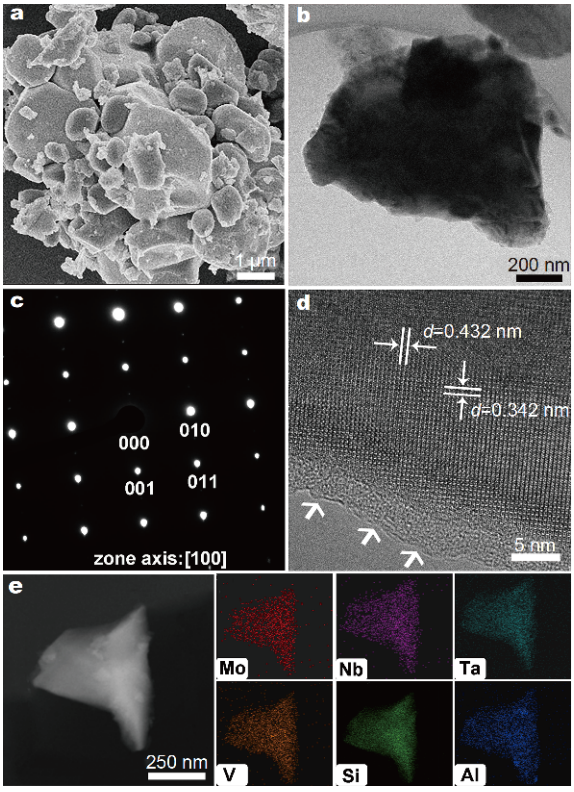


**Figure 3** SEM and TEM analysis of the as-synthesized HEAS-1. (a) SEM image; (b) TEM image; (c) SAED pattern; (d) HRTEM image; (e) STEM image and corresponding EDS compositional maps.

formation possibility of HEAS-1 by analyzing lattice size difference and chemical reaction thermodynamics based on first-principles calculations and then successfully fabricated HEAS-1 by solid-state reaction at 1573 K for the first time. The as-synthesized HEAS-1 exhibited the single-crystal hexagonal *C*40 crystal structure with the space group of $P6_222$. More importantly, the distribution of all elements including the cation elements (Mo, Nb, Ta and V) and the anion elements (Al and Si) is highly uniform without evident localization or segregation in the as-synthesized HEAS-1.

**Received 13 July 2019; accepted 14 August 2019; published online 19 September 2019**


1 Miracle DB, Senkov ON. A critical review of high entropy alloys and related concepts. Acta Mater, 2017, 122: 448–511
2 Tsai MH, Yeh JW. High-entropy alloys: a critical review. Mater Res Lett, 2014, 2: 107–123
3 Zhang W, Liaw PK, Zhang Y. Science and technology in high-entropy alloys. Sci China Mater, 2018, 61: 2–22
4 Shi P, Ren W, Zheng T, *et al.* Enhanced strength-ductility synergy in ultrafine-grained eutectic high-entropy alloys by inheriting microstructural lamellae. Nat Commun, 2019, 10: 489
5 El-Atwani O, Li N, Li M, *et al.* Outstanding radiation resistance of tungsten-based high-entropy alloys. Sci Adv, 2019, 5: eaav2002
6 Shi Y, Yang B, Xie X, *et al.* Corrosion of $Al_x$CoCrFeNi high-entropy alloys: Al-content and potential scan-rate dependent pitting behavior. Corros Sci, 2017, 119: 33–45
7 Zhang ZJ, Mao MM, Wang J, *et al.* Nanoscale origins of the damage tolerance of the high-entropy alloy CrMnFeCoNi. Nat Commun, 2015, 6: 10143
8 Chen S, Li W, Xie X, *et al.* Nanoscale serration and creep characteristics of $Al_{0.5}$CoCrCuFeNi high-entropy alloys. J Alloys Compd, 2018, 752: 464–475
9 Niu S, Kou H, Zhang Y, *et al.* The characteristics of serration in $Al_{0.5}$CoCrFeNi high entropy alloy. Mater Sci Eng-A, 2017, 702: 96–103
10 Rost CM, Sachet E, Borman T, *et al.* Entropy-stabilized oxides. Nat Commun, 2015, 6: 8485
11 Jiang S, Hu T, Gild J, *et al.* A new class of high-entropy perovskite oxides. Scripta Mater, 2018, 142: 116–120
12 Harrington TJ, Gild J, Sarker P, *et al.* Phase stability and mechanical properties of novel high entropy transition metal carbides. Acta Mater, 2019, 166: 271–280
13 Ye B, Wen T, Huang K, *et al.* First-principles study, fabrication, and characterization of $(Hf_{0.2}Zr_{0.2}Ta_{0.2}Nb_{0.2}Ti_{0.2})C$ high-entropy ceramic. J Am Ceram Soc, 2019, 102: 4344–4352
14 Ye B, Wen T, Nguyen MC, *et al.* First-principles study, fabrication and characterization of $(Zr_{0.25}Nb_{0.25}Ti_{0.25}V_{0.25})C$ high-entropy ceramics. Acta Mater, 2019, 170: 15–23
15 Feng L, Fahrenholtz WG, Hilmas GE, *et al.* Synthesis of single-phase high-entropy carbide powders. Scripta Mater, 2019, 162: 90–93
16 Ye B, Ning S, Liu D, *et al.* One-step synthesis of coral-like high-entropy metal carbide powders. J Am Ceram Soc, 2019, 102: 6372–6378
17 Gild J, Zhang Y, Harrington T, *et al.* High-entropy metal diborides: a new class of high-entropy materials and a new type of ultrahigh temperature ceramics. Sci Rep, 2016, 6: 37946
18 Tallarita G, Licheri R, Garroni S, *et al.* Novel processing route for the fabrication of bulk high-entropy metal diborides. Scripta Mater, 2019, 158: 100–104
19 Liu D, Wen T, Ye B, *et al.* Synthesis of superfine high-entropy metal diboride powders. Scripta Mater, 2019, 167: 110–114
20 Gild J, Braun J, Kaufmann K, *et al.* A high-entropy silicide: $(Mo_{0.2}Nb_{0.2}Ta_{0.2}Ti_{0.2}W_{0.2})Si_2$. J Materiomics, 2019, doi: 10.1016/j.jmat.2019.03.002
21 Qin Y, Liu JX, Li F, *et al.* A high entropy silicide by reactive spark plasma sintering. J Adv Ceram, 2019, 8: 148–152
22 Ye B, Wen T, Liu D, *et al.* Oxidation behavior of $(Hf_{0.2}Zr_{0.2}Ta_{0.2}Nb_{0.2}Ti_{0.2})C$ high-entropy ceramics at 1073–1473 K in air. Corros Sci, 2019, 153: 327–332
23 Ye B, Wen T, Chu Y. High-temperature oxidation behavior of $(Hf_{0.2}Zr_{0.2}Ta_{0.2}Nb_{0.2}Ti_{0.2})C$ high-entropy ceramics in air. J Am Ceram Soc, 2019, 122: jace.16725
24 Kresse G, Furthmüller J. Efficient iterative schemes for *ab initio* total-energy calculations using a plane-wave basis set. Phys Rev B, 1996, 54: 11169–11186
25 Kresse G, Hafner J. *Ab initio* molecular dynamics for liquid metals. Phys Rev B, 1993, 47: 558–561
26 Blöchl PE. Projector augmented-wave method. Phys Rev B, 1994, 50: 17953–17979
27 Perdew JP, Burke K, Ernzerhof M. Generalized gradient approximation made simple. Phys Rev Lett, 1996, 77: 3865–3868
28 Jain A, Ong SP, Hautier G, *et al.* Commentary: the materials project: a materials genome approach to accelerating materials innovation. APL Mater, 2013, 1: 011002
29 Zunger A, Wei SH, Ferreira LG, *et al.* Special quasirandom structures. Phys Rev Lett, 1990, 65: 353–356
30 van de Walle A. Multicomponent multisublattice alloys, nonconfigurational entropy and other additions to the alloy theoretic automated toolkit. Calphad, 2009, 33: 266–278


**Acknowledgements** This work was supported by the National Key Research and Development Program of China (2017YFB0703200), Young Elite Scientists Sponsorship Program by China Association for Science and Technology (2017QNRC001), and the National Natural Science Foundation of China (51802100 and 51972116).

**Author contributions** Chu Y conceived and designed the experiments. Chu Y and Liu H performed the experiments. Chu Y, Wen T, Liu H, Ye B and Liu D analyzed the data. Wen T performed the first-principles calculations. All authors commented on the manuscript.

**Conflict of interest** The authors declare that they have no conflict of interest.

  

**Tongqi Wen** is currently a PhD student at Northwestern Polytechnical University and jointly supervised in Ames laboratory, USA and South China University of Technology. His research interests include computational modeling, crystal structure prediction and materials discovery.

**Honghua Liu** is currently a Master student at South China University of Technology. His research focuses on the fabrication and characterization of high-entropy ceramics and related powders.

**Yanhui Chu** is as an associate professor at South China University of Technology. He received his PhD degree in materials science from Northwestern Polytechnical University in 2016. From January 2014 to August 2015, he was a visiting scholar at Harvard University. His current research interests include high-temperature coatings, high-entropy ceramics and related nanomaterials.

## 高熵硅铝化物: 一类新型的高熵陶瓷材料

文通其[1,2†], 刘红华[1†], 叶贝琳[1], 刘达[1], 褚衍辉[1*]

**摘要** 高熵陶瓷材料因具有巨大的组分空间、独特的微观结构以及可调控的性能而引起国内外研究者的广泛关注. 目前, 高熵陶瓷材料的研究主要集中在具有多主元阳离子结构的高熵陶瓷材料领域. 然而, 关于具有多主元阴阳离子结构的高熵陶瓷材料的研究报道较少. 本文首次报道了一类新型的具有多主元阴阳离子结构的高熵陶瓷材料, 即高熵硅铝化物$(Mo_{0.25}Nb_{0.25}Ta_{0.25}V_{0.25})(Al_{0.5}Si_{0.5})_2$. 首先基于第一性原理计算从化学反应热力学和晶格尺寸差异两个方面分析了高熵硅铝化物形成的可能性, 然后以过渡金属粉体以及硅粉和铝粉为原料, 采用固相反应技术在1573 K下成功地制备出等摩尔比的高熵硅铝化物. 研究结果表明: 所制备的高熵硅铝化物具有单一金属硅铝化物的六方晶系晶体结构, 同时, 所有组成元素的分布具有高度均匀性. 该研究不仅丰富了高熵陶瓷材料的种类, 而且为开拓具有多主元阴阳离子结构的高熵陶瓷材料提供了参考.